



Increased local expression of coagulation factor X contributes to the fibrotic response in human and murine lung injury

Chris J. Scotton,¹ Malvina A. Krupiczkoj,¹ Melanie Königshoff,² Paul F. Mercer,¹ Y.C. Gary Lee,¹ Naftali Kaminski,³ John Morser,⁴ Joseph M. Post,⁴ Toby M. Maher,¹ Andrew G. Nicholson,⁵ James D. Moffatt,¹ Geoffrey J. Laurent,¹ Claudia K. Derian,⁶ Oliver Eickelberg,² and Rachel C. Chambers¹

¹Centre for Respiratory Research, University College London, London, United Kingdom. ²Department of Internal Medicine II, University of Giessen Lung Centre, Giessen, Germany. ³Dorothy P. and Richard P. Simmons Center for Interstitial Lung Diseases, University of Pittsburgh Medical Center, Pittsburgh, Pennsylvania, USA. ⁴Berlex Biosciences, Richmond, California, USA. ⁵Department of Histopathology, Royal Brompton and Harefield Hospitals, NHS Foundation Trust, and National Heart and Lung Division, Imperial College London, London, United Kingdom. ⁶Johnson & Johnson Pharmaceutical Research and Development, Spring House, Pennsylvania, USA.

Uncontrolled activation of the coagulation cascade contributes to the pathophysiology of several conditions, including acute and chronic lung diseases. Coagulation zymogens are considered to be largely derived from the circulation and locally activated in response to tissue injury and microvascular leak. Here we report that expression of coagulation factor X (FX) is locally increased in human and murine fibrotic lung tissue, with marked immunostaining associated with bronchial and alveolar epithelia. FXa was a potent inducer of the myofibroblast differentiation program in cultured primary human adult lung fibroblasts via TGF- β activation that was mediated by proteinase-activated receptor-1 (PAR1) and integrin $\alpha_v\beta_5$. PAR1, $\alpha_v\beta_5$, and α -SMA colocalized to fibrotic foci in lung biopsy specimens from individuals with idiopathic pulmonary fibrosis. Moreover, we demonstrated a causal link between FXa and fibrosis development by showing that a direct FXa inhibitor attenuated bleomycin-induced pulmonary fibrosis in mice. These data support what we believe to be a novel pathogenetic mechanism by which FXa, a central proteinase of the coagulation cascade, is locally expressed and drives the fibrotic response to lung injury. These findings herald a shift in our understanding of the origins of excessive procoagulant activity and place PAR1 central to the cross-talk between local procoagulant signaling and tissue remodeling.

Introduction

The primary function of the coagulation cascade is to promote hemostasis and limit blood loss in response to tissue injury. However, it is now recognized that the physiological functions of the coagulation cascade extend beyond blood coagulation and that this cascade plays a pivotal role in influencing inflammatory and repair responses to tissue injury. Consequently, uncontrolled coagulation activity contributes to the pathophysiology of several conditions, including thrombosis, arthritis, cancer, kidney disease, inflammatory bowel disease, and acute and chronic lung injury (1–5). In all of these disease states, it is still generally held that coagulation zymogens are principally synthesized in the liver and released into the circulation as inactive precursors that are only activated as a consequence of the initiation of the tissue factor-dependent (TF-dependent) coagulation pathway at sites of injury (6).

How coagulation proteinases, such as thrombin, influence cellular responses was elucidated by the discovery of the proteinase-activated receptors (PARs) in the early 1990s (7). There are currently 4 known members of the PAR family, PAR1–PAR4, which are activated, as their name suggests, by a unique mechanism involving limited proteolysis leading to the unmasking of a

ligand tethered to the receptor. Collectively, the proteinases of the coagulation cascade can target all 4 family members. Thrombin is considered to be a major activator of PAR1, PAR3, and PAR4, whereas factor Xa (FXa), either on its own or as part of the more potent TF/FVIIa/FXa ternary complex, activates either PAR1 or PAR2, depending on cell type and cofactor expression (8–10).

In this study, we focused on the role of procoagulant signaling in the fibroproliferative response to lung injury, in which the normal lung parenchyma is progressively replaced with fibrous tissue, and for which uncontrolled coagulation activity is increasingly thought to be of paramount importance. Both thrombin and coagulation FXa are elevated in BAL fluid (BALF) obtained from patients with acute lung injury (ALI) and pulmonary fibrosis (3, 11, 12). Consequently, extravascular intra-alveolar accumulation of fibrin is commonly observed in the lungs of patients with ALI and acute respiratory distress syndrome (ARDS; ref. 3), the most severe form of ALI, in which rapid fibroproliferation often leads to the development of extensive fibrotic lesions (13). Fibrin deposition has also been reported in the lungs of patients with chronic fibrotic lung diseases, including systemic sclerosis and idiopathic pulmonary fibrosis (IPF; ref. 14); a recent small, nonblinded study showed that anticoagulant therapy may hold some promise for patients with IPF (15). Moreover, we and others have shown that PAR1, the major high-affinity signaling receptor for thrombin, is highly expressed by fibroblasts within fibrotic foci in the lungs of patients with these conditions (16, 17) and that modulation of

Authorship note: Chris J. Scotton and Malvina A. Krupiczkoj contributed equally to this work.

Conflict of interest: The authors have declared that no conflict of interest exists.

Citation for this article: *J. Clin. Invest.* 119:2550–2563 (2009). doi:10.1172/JCI33288.

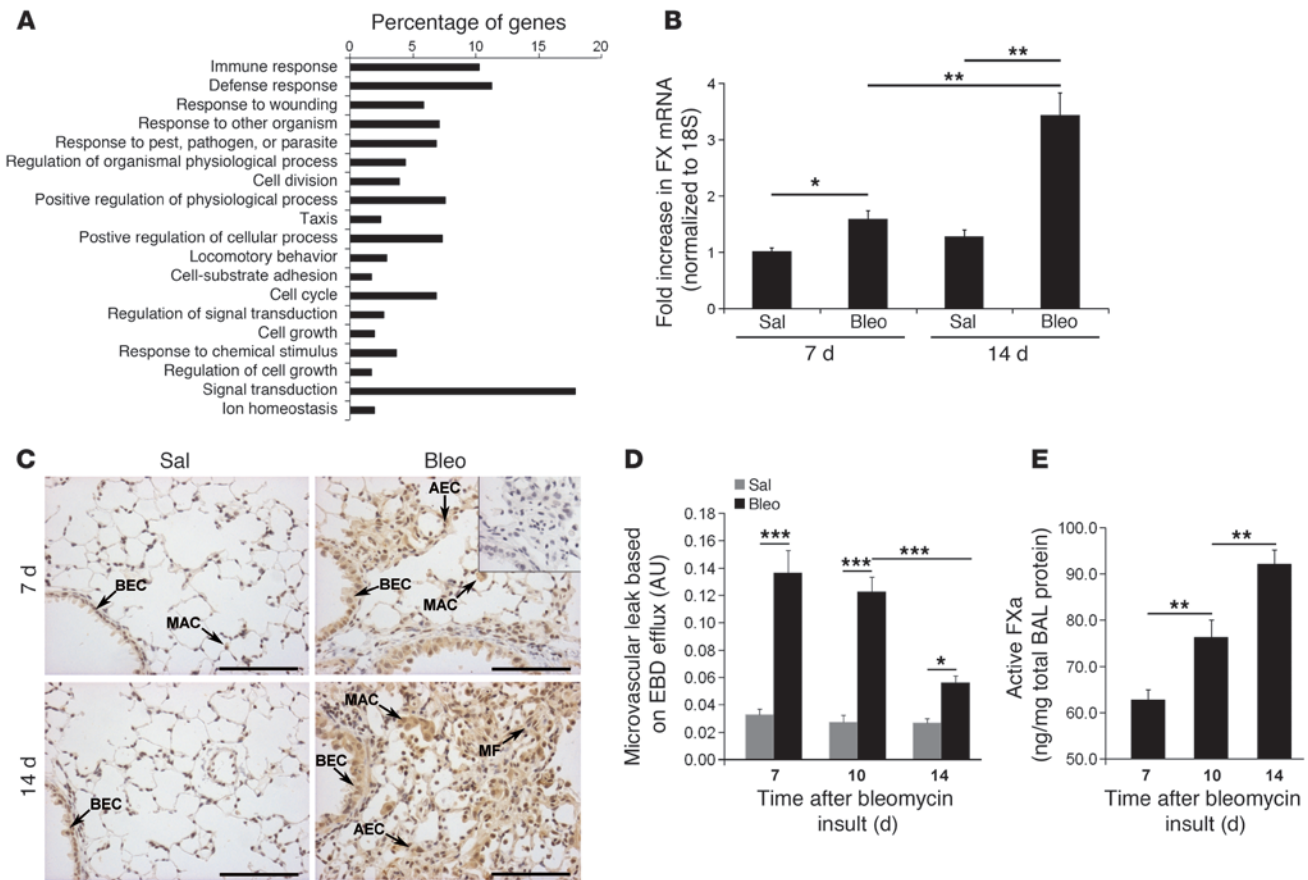


Figure 1

Bleomycin-induced lung injury increases local expression of FX/FXa in the murine lung. **(A)** Functional annotation analysis of the genes regulated in mice 14 days after bleomycin instillation, showing the percentage of genes statistically overrepresented within each gene ontology category, arranged in descending order of significance. **(B)** FX mRNA levels in mouse lung homogenates at 7 and 14 days after saline (Sal; $n = 3$) or bleomycin (Bleo; $n = 5$), as assessed by real-time RT-PCR. Data are mean \pm SEM. **(C)** Photomicrographs of representative histological sections showing FX/FXa immunoreactivity in mouse lungs 7 and 14 days after saline or bleomycin ($n = 4$ per group). Immunostaining increased in bleomycin-instilled mice and localized mainly to alveolar (AEC) and bronchial (BEC) epithelial cells as well as alveolar macrophage (MAC) and myofibroblasts (MF) in fibrotic foci. Inset shows an IgG isotype control section, revealing no apparent staining (original magnification, $\times 200$). Scale bars: 100 μm . **(D)** Microvascular leak was determined by efflux of intravenously injected EBD into BALF. Data are mean \pm SEM ($n = 5$ per group). **(E)** Active FXa levels in BALF were determined by chromogenic assay. Data are mean \pm SEM ($n = 5$ per group). * $P < 0.05$, ** $P < 0.01$, *** $P < 0.001$, ANOVA.

procoagulant activity within the alveolar compartment attenuates experimental lung fibrosis (18–20). We have further shown that PAR1 deficiency affords protection from bleomycin-induced lung inflammation and fibrosis (16). PAR1 blockade is also protective in experimental liver fibrosis (21), so this receptor may play a central role in the cross-talk between coagulation and tissue remodeling in a broad range of conditions.

We used global expression profiling during the fibroproliferative response to bleomycin injury in mice to gain insights into the mechanism by which the coagulation pathway drives the fibrotic response to lung injury. To our knowledge, we are the first to show that FX, a central proteinase of the coagulation pathway, was locally produced in the murine and human fibrotic lung and that direct FXa inhibition afforded protection from bleomycin-induced lung collagen accumulation. We further show that FXa induced fibroblast to myofibroblast differentiation via a PAR1-dependent signaling mechanism. These observations provide a marked shift in our

understanding of the cellular origin of excessive coagulation activity in lung injury. We propose that FXa, derived from a local tissue source rather than from the circulation, may represent an important physiological activator of PAR1 in extravascular compartments in the absence of ongoing injury and microvascular leak.

Results

FX is upregulated in bleomycin-induced lung injury. Global expression profiling by microarray analysis revealed the regulation of 399 nonredundant genes 14 days after bleomycin challenge in C57BL/6J mice; 292 genes were upregulated with a fold change greater than 2, and 107 genes were downregulated (for full list of genes, see Supplemental Table 1; supplemental material available online with this article; doi:10.1172/JCI33288DS1). Functional annotation analysis of these genes revealed that the statistically overrepresented themes of the list tended toward a response to injury (Figure 1A), as might be expected after bleomycin challenge.

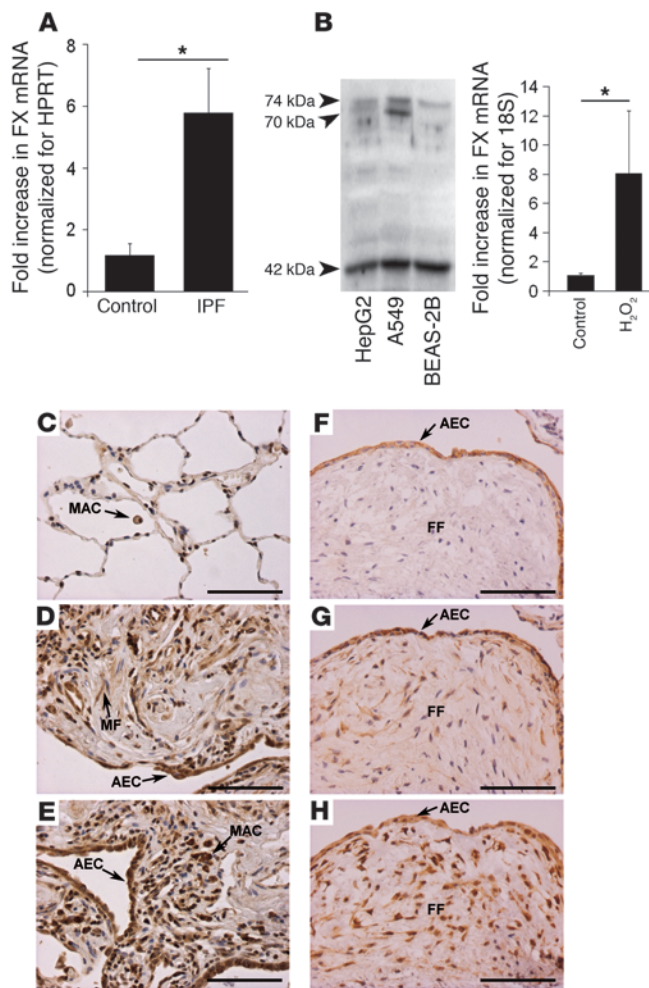


Figure 2

FX expression is locally upregulated in the human UIP lung. (A) FX expression in microdissected alveolar septae from human IPF and donor lungs, analyzed by real-time RT-PCR. Data are mean \pm SEM ($n = 4$ patients per group). (B) FX was expressed by HepG2, A549, and BEAS-2B cells in vitro, as demonstrated by Western blot. FX mRNA expression in A549 was upregulated by 1 hour treatment with 400 μ M H_2O_2 . Data are mean \pm SEM, representative of 3 independent experiments. (C–E) Photomicrographs of representative histological sections showing FX/FXa immunolocalization in the lung biopsy specimens of the Brompton cohort. (C) Weak staining was observed in normal control biopsy tissue ($n = 6$), which mainly localized to alveolar macrophages. (D and E) A marked increase in staining was observed in fibrotic biopsy specimens ($n = 7$), localized mainly to alveolar epithelial cells, but also to macrophages and myofibroblasts in fibrotic foci. (F–H) Photomicrographs of TF (F), FVII/FVIIa (G), and FX/FXa (H) in serial sections, showing colocalization of all 3 to alveolar epithelium overlying fibrotic foci (FF). Fibroblasts within fibrotic foci were also strongly immunoreactive for FX/FXa. Scale bars: 100 μ m. * $P = 0.005$, Student's t test.

animals greater than 4-fold over that of saline-control animals at 7 and 10 days, during the inflammatory phase of the bleomycin response (Figure 1D). However, by 14 days, during the fibrotic phase of the response, microvascular leak almost completely subsided to control levels (Figure 1D).

FXa activity in BALF was determined using a highly specific chromogenic assay. In saline-control animals, FXa activity was undetectable. After bleomycin-induced lung injury, active FXa enzyme was measurable in BALF at all time points examined, and the proportion of active FXa in total BALF protein increased during the fibrotic phase of the bleomycin response (Figure 1E). Taken together, these data demonstrate that microvascular leak subsided during the fibrotic phase of the bleomycin response, while FXa activity was maintained, coincident with the peak in local expression of FX mRNA. These observations suggest that local FX production likely contributes to the intra-alveolar pool of FXa activity during the fibrotic phase.

FX is upregulated in IPF. To determine whether our findings in the bleomycin model translate to human fibrotic lung disease, we analyzed FX mRNA levels in lung biopsy specimens from IPF ($n = 4$) or control ($n = 4$) patients. FX mRNA was detectable in total lung homogenates, but there was no significant difference between control and fibrotic lung (data not shown). In contrast, there was a marked 5-fold increase in FX mRNA levels in samples obtained from laser-capture microdissected alveolar septae of patients with IPF compared with the corresponding areas from control lung tissue (Figure 2A).

The ability of lung epithelial cells to produce FX at the mRNA and protein levels was then confirmed in vitro in A549 and BEAS-2B cells (Figure 2B). The FX protein produced by these cell lines migrated as 3 bands of 74, 70, and 42 kDa in a fashion identical to that observed for the hepatocyte cell line HepG2 (Figure 2B). The molecular weights of these bands were consistent with those reported for the heavy chain of FX in both the preprotein and processed conformations (26). Interestingly, our gene chip studies further revealed that the enzymes γ -carboxylase, which is essential for γ -carboxylation of the zymogen, and Vitamin K epoxide reductase, which is essential for Vitamin K reduction after it has been oxidized in the carboxylation of glutamic acid (27), were both expressed in the lung (data not shown). Alveolar macrophages (obtained from BAL) and cultured primary human adult lung

Many of the regulated genes had previously been identified from microarray analysis of the bleomycin model (22–25), including collagen I, fibronectin, MMP-12, and PDGF. However, to our surprise, one of the highly upregulated genes included FX, with 5-fold upregulation at 14 days compared with saline-treated mice.

We next confirmed the expression of FX in the bleomycin model of fibrosis by real-time RT-PCR and found that FX mRNA levels increased significantly, by 1.6-fold at 7 days and by 3.5-fold at 14 days (Figure 1B). Immunolocalization studies with an antibody that recognizes FX/FXa confirmed that there was a strong signal for this protein in bleomycin-injured lungs at 7 and 14 days (Figure 1C) compared with the weak signal observed for saline control lungs. Bronchial and alveolar epithelial cells showed the most positive signal, but infiltrating macrophages and myofibroblasts within fibrotic areas were also immunoreactive.

Current dogma assumes that this FX immunoreactivity is derived solely from the circulating pool of FX protein through microvascular leak, rather than from local production. We therefore tracked the kinetics of lung barrier permeability and BALF FXa activity in response to bleomycin injury in order to clarify the relationship between extravascular FXa and microvascular leak. Barrier permeability was assessed by measuring efflux of intravenously injected Evans blue dye (EBD) into the alveolar space (sampled by BAL). As expected, microvascular leak increased in bleomycin-injured

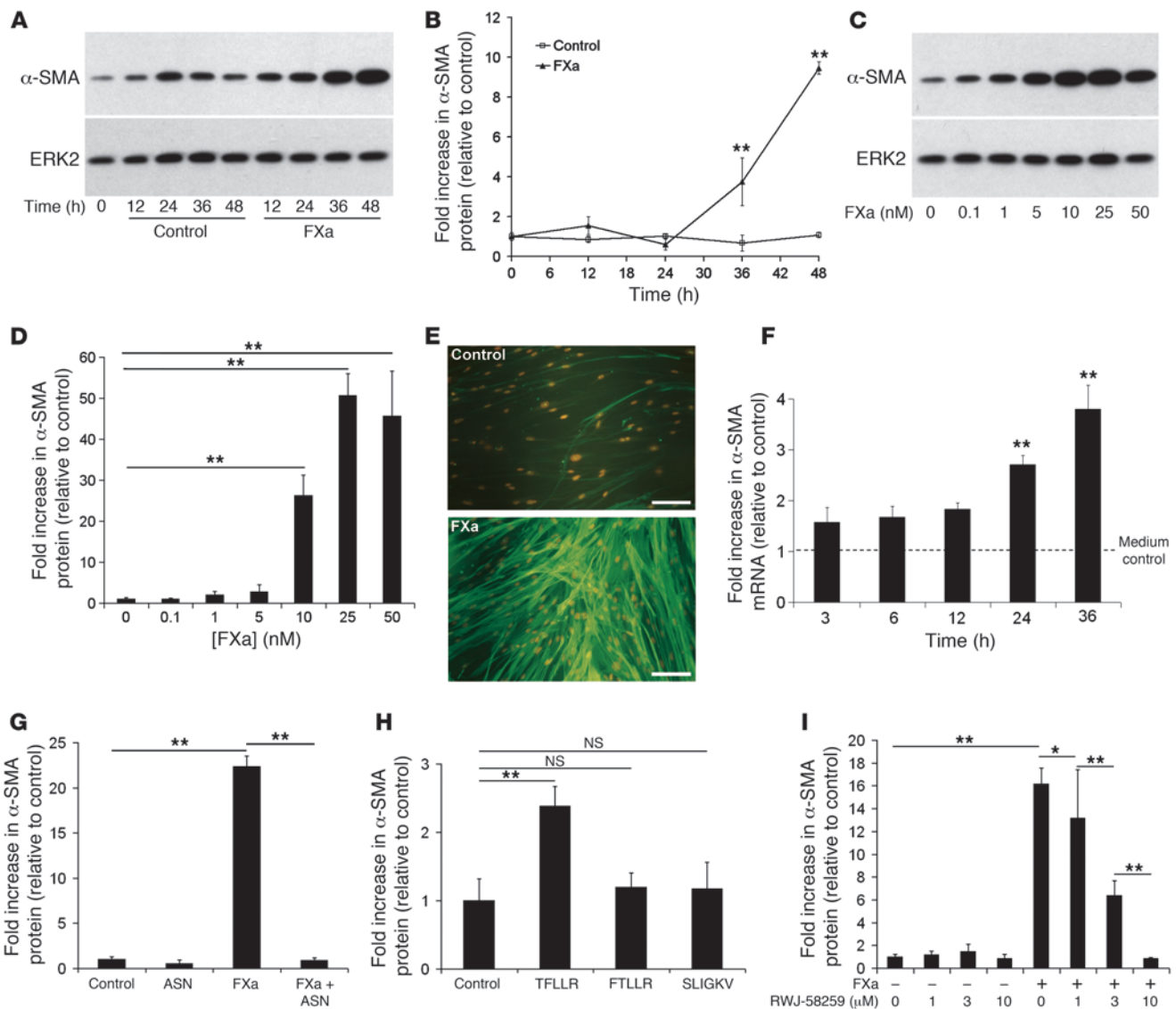


Figure 3

FXa induces fibroblast-to-myfibroblast differentiation via activation of PAR1, but not of PAR2. (A and B) Time response of FXa-induced α -SMA protein expression in pHALFs. (A) Representative immunoblot for α -SMA and ERK2 loading control. (B) Quantification by densitometry. (C and D) Dose response of FXa-induced α -SMA protein expression. (C) Representative immunoblots. (D) Quantification by densitometry. (E) Immunocytofluorescence demonstrating α -SMA stress fiber formation in pHALFs after FXa exposure for 36 hours. Scale bars: 40 μ m. (F) Effect of FXa stimulation on α -SMA mRNA expression in pHALFs, analyzed by real-time RT-PCR. (G) Effect of antistasin (ASN) on FXa-induced α -SMA protein expression, measured by Western blotting. (H) Effect of synthetic peptide agonists for PAR1 (TFLLR-NH₂, 200 μ M), PAR2 (SLIGKV-NH₂, 200 μ M) and scrambled peptide control (FTLLR-NH₂, 200 μ M) on α -SMA protein expression. (I) Effect of the selective PAR1 antagonist RWJ-58259 on FXa-induced α -SMA protein expression. Data are mean \pm SD, representative of 3 separate experiments with 3 replicates per experimental group. * P < 0.05, ** P < 0.001, ANOVA.

fibroblasts (pHALFs) did not express FX in vitro (data not shown), which suggests that epithelial cells are the sole source of the FX mRNA signal in vivo.

To begin examining the mechanism by which FX is upregulated, we investigated the effect of various proinflammatory and profibrotic mediators implicated in the pathogenesis of IPF on FX mRNA and protein expression in vitro. TGF- β , IL-1 β , TNF- α , and IL-13 had no effect on FX expression (data not shown). However, oxidative stress induced by 50 U/ml bleomycin treatment significantly increased FX mRNA levels in A549 cells after as little as

1 hour stimulation, with a peak of 6.4-fold at 24 hours (P = 0.004; data not shown). Similarly, exposure of A549 cells to 400 μ M H₂O₂ resulted in significantly increased FX mRNA levels after 1 hour (Figure 2B), and treatment with superoxide (generated from the reaction between xanthine and xanthine oxidase) also increased FX gene expression (data not shown). These data suggest that oxidative stress may be an important mechanism by which local FX expression is increased in the fibrotic lung.

Immunohistochemical studies of the Brompton cohort, composed of 7 patients with IPF and 6 control lungs, confirmed the



strong upregulation of FX/FXa in IPF lungs that was associated with the bronchial and alveolar epithelium and also with infiltrating macrophages and myofibroblasts within fibrotic foci (Figure 2, D and E). Weak staining was observed in control biopsy tissue, mainly localized to alveolar macrophages (Figure 2C). The immunostaining pattern was confirmed in human tissue microarrays taken from the Pittsburgh cohort of IPF and control lung biopsy samples ($n = 18$; data not shown). To determine whether the fibrotic lung can convert FX to its active form via assembly of the TF/FVIIa/FX ternary complex of the extrinsic coagulation pathway, we investigated the immunolocalization of TF, FVII, and FX in serial histological sections. Whereas TF immunostaining was confined to the alveolar epithelium overlying fibrotic foci, as was previously reported (14), FVII and FX/FXa immunoreactivity exhibited a more diffuse staining pattern – with clear colocalization with TF on the alveolar epithelium – but also considerable staining on fibroblasts within the fibrotic foci (Figure 2, F–H). This staining pattern lends strong support to the notion that the TF/FVIIa/FX ternary complex may assemble on the alveolar epithelium, allowing activation of FX to FXa – which in turn interacts with fibroblasts within the underlying fibrotic regions.

FXa induces myofibroblast differentiation via PAR1. Fibroblast-to-myofibroblast differentiation is central to the pathogenesis of pulmonary fibrosis (28). To examine whether FXa signaling promotes this differentiation program, we examined the effect of FXa on the de novo expression of the myofibroblast marker protein α -SMA by cultured pHALFs. Western blotting revealed that FXa induced α -SMA expression in a concentration- and time-dependent manner, with levels increased by 50-fold at 25 nM (Figure 3, A–D). This response was not immediate, with the earliest increase detected at 24 hours at the mRNA level (Figure 3F) and at 36 hours at the protein level (Figure 3, A and B). The ability of FXa to induce α -SMA protein expression was confirmed in other cell types, including human fetal lung fibroblasts (HFL-1) and in murine lung fibroblasts (MLFs; Supplemental Figure 1A). Immunocytofluorescence microscopy confirmed that FXa induced the assembly of an extensive network of α -SMA stress fibers in greater than 90% of cells after 36 hours (Figure 3E).

To exclude the possibility that FXa exerts these effects via the activation of any prothrombin in the culture media, we assessed α -SMA protein induction in the presence of the specific thrombin inhibitor hirudin (Supplemental Figure 1B). Hirudin completely inhibited α -SMA protein expression induced by thrombin, but exerted a minor effect on FXa-induced α -SMA protein expression. In contrast, the potent and selective FXa proteolytic inhibitor antistasin (29) completely blocked FXa-induced α -SMA protein levels (Figure 3G).

We next sought to determine the receptor mechanism by which FXa induces myofibroblast differentiation. RT-PCR studies revealed that pHALFs expressed the FXa signaling receptors PAR1 and PAR2 (data not shown). The specific PAR1-activating peptide TFLLR-NH₂, used at a standard concentration, significantly increased α -SMA protein levels, but was less efficient than FXa (Figure 3H). The scrambled PAR1 control peptide FTLLR-NH₂ and the PAR2-activating peptide SLIGKV-NH₂ had no effect. Preincubation of cells with the potent and selective PAR1 antagonist RWJ-58259 (30, 31) inhibited FXa-induced α -SMA protein expression in a dose-dependent manner, with levels completely blocked at the highest concentration tested (Figure 3I).

Because PAR1 couples to multiple members of the G protein family (32), the effect of pertussis toxin (PTX) and the PAR1-G α_q

inhibitor Q94 (see Methods) on FXa-induced α -SMA expression was also assessed. Preincubation of pHALFs with 100 ng/ml PTX to block receptor coupling to G α_i had no inhibitory effect on α -SMA levels (data not shown). However, Q94, which selectively blocks the interaction of PAR1 with G α_q , caused a concentration-dependent blockade of FXa-induced α -SMA induction (0.1 μ M, 27%; 10 μ M, 93%; $P < 0.001$; data not shown). These data further supported our findings using the PAR1 antagonist RWJ-58259 that FXa induced α -SMA mRNA and protein levels in pHALFs via activation of PAR1, not PAR2, and moreover demonstrated that PAR1 coupling to G α_q was necessary for the response.

FXa induces α -SMA expression via a TGF- β -dependent mechanism. We next determined whether FXa exerts its effects via production and/or activation of a secondary mediator, such as TGF- β , which is known to induce fibroblast differentiation (33). FXa stimulation of pHALFs did not influence TGF- β_1 and TGF- β_2 mRNA levels (data not shown). The activation of latent TGF- β is the major rate-limiting step in TGF- β bioavailability. We therefore determined whether FXa stimulation activates latent TGF- β . Active TGF- β levels were initially assessed using a bioassay based on a fibroblast-transformed mink lung epithelial reporter cell (tMLEC) coculture system, in which fibroblast-derived active TGF- β is detected by tMLEC reporter cells expressing luciferase under the control of the TGF- β -responsive plasminogen activator inhibitor-1 (PAI-1) promoter (34). For these experiments, we used TFLLR-NH₂ in order to avoid extraneous results caused by the proteolytic activity of FXa in this bioassay. Figure 4A shows that TFLLR-NH₂ increased tMLEC luciferase activity, and this activity was completely inhibited by the pan-specific TGF- β -neutralizing antibody 1D11. Taken together, these data indicate that PAR1 activation alone is sufficient for TGF- β activation in pHALFs.

TGF- β signals in fibroblasts via the formation of a heterotetrameric receptor complex composed of a TGF- β type 2 receptor dimer with an activin-like kinase 5 (ALK5) TGF- β type 1 receptor dimer; this in turn triggers the SMAD signaling pathway by phosphorylating SMAD2 and SMAD3. We examined the effect of FXa on SMAD2/3 phosphorylation by pHALFs in monoculture and found that FXa increased levels of phospho-SMAD2/3 (pSMAD2/3) at 6 and 10 hours after stimulation (Figure 4, B and C), corroborating the findings of the TGF- β bioassay.

We next examined the involvement of TGF- β signaling in FXa-induced myofibroblast differentiation using 2 pharmacologically unrelated selective small-molecule inhibitors of ALK5: SB431542 and SD-208. Figure 4, D and E, shows that both compounds inhibited FXa-induced α -SMA protein expression in a concentration-dependent manner, with complete inhibition achieved at 10 μ M SB431542 (Figure 4D) and 0.1 μ M SD-208 (Figure 4E). At these concentrations, the inhibitors also fully blocked α -SMA protein induction by exogenously added TGF- β (data not shown). SB431542 also blocked α -SMA induction by 10 nM thrombin (data not shown), which indicates that this coagulation proteinase also leads to myofibroblast differentiation via TGF- β signaling.

TGF- β activation is dependent on the dissociation of TGF- β from the TGF- β latency-associated peptide (LAP). Depending on the cell type, this may be mediated by proteolytic cleavage (e.g., by MMPs) or by the proteolytic-independent interaction of LAP with integrins (e.g., $\alpha_v\beta_3$, $\alpha_v\beta_5$, and $\alpha_v\beta_6$) or the matrix glycoprotein thrombospondin-1 (TSP-1; reviewed in refs. 35, 36). Our initial investigations demonstrated that FXa induced a time-dependent increase in TSP-1 mRNA and protein levels (Supplemental Figure 1, C–E). TSP-1

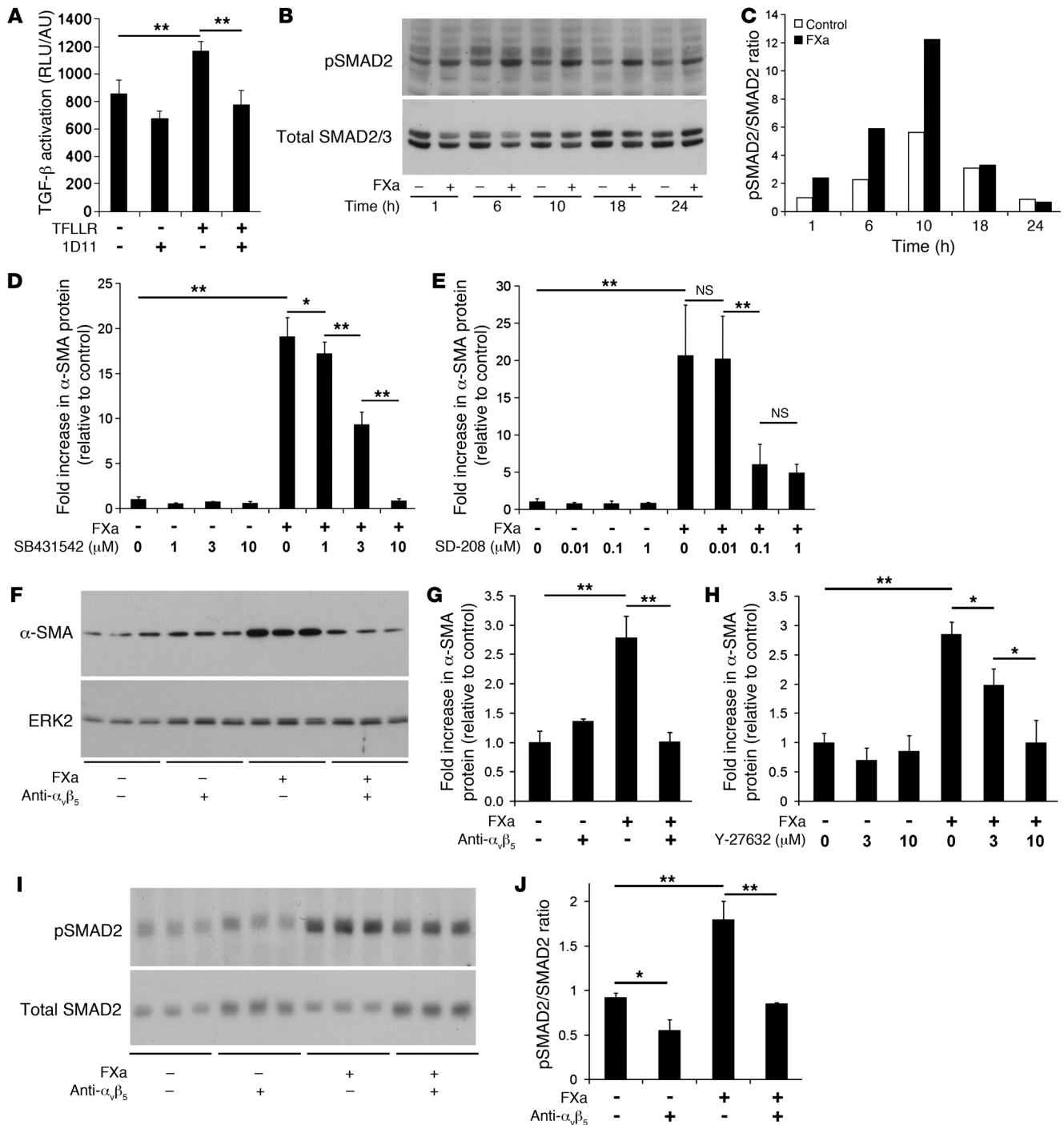


Figure 4

FXa-induced α -SMA protein expression is dependent on TGF- β activity. (A) Effect of TFLLR-NH₂ on TGF- β activation. pHALFs were grown in coculture with tMLECs (see Methods). Activation was blocked by the pan-specific TGF- β -neutralizing antibody 1D11. (B and C) Time course of SMAD2 phosphorylation by FXa. (B) Representative immunoblot for pSMAD2 and total SMAD2/3 loading control. (C) Densitometric analysis. (D and E) Effect of ALK5 inhibition with SB431542 (D) and SD-208 (E) on FXa-induced α -SMA protein expression, analyzed by Western blotting. Cell cultures were preincubated with inhibitors for 30 minutes prior to 36 hours FXa exposure. Densitometric analyses are shown. (F and G) Effect of $\alpha_v\beta_3$ -neutralizing antibodies on FXa-induced α -SMA protein expression. Cell cultures were preincubated with 10 μ g/ml anti- $\alpha_v\beta_3$ or isotype control antibody for 1 hour prior to 36 hours FXa exposure. (F) Representative immunoblots for α -SMA and ERK2 loading control. (G) Densitometric analysis (mean \pm SEM). (H) Effect of Y-27632 on FXa-induced α -SMA protein expression. Cell cultures were preincubated with Y-27632 for 1 hour prior to 36 hours FXa exposure; densitometric analysis is shown (mean \pm SEM). (I and J) Effect of $\alpha_v\beta_3$ -neutralizing antibodies on FXa-induced SMAD2 phosphorylation. Cell cultures were preincubated with 10 μ g/ml anti- $\alpha_v\beta_3$ or isotype control antibody for 1 hour prior to 10 hours FXa exposure. (I) Representative immunoblots. (J) Densitometric analysis, representative of 2 separate experiments (mean \pm SEM). Unless otherwise indicated, data (mean \pm SD) are representative of 3 separate experiments, with 3 replicates per group. * P < 0.05, ** P < 0.001, ANOVA.

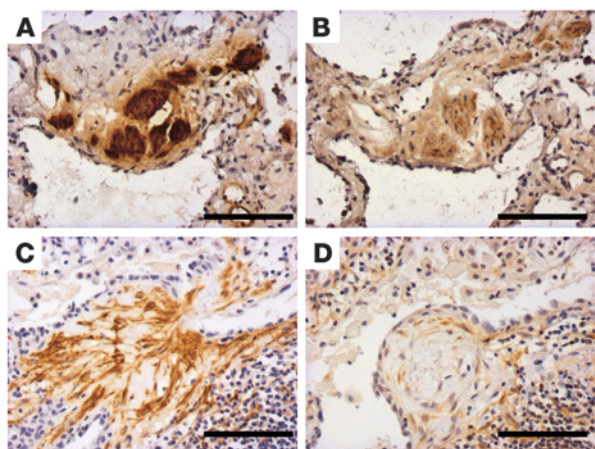


Figure 5

Immunolocalization of α -SMA, $\alpha_v\beta_5$, and PAR1 in human IPF lung. (A and B) Photomicrographs of representative 3- μ m serial cryostat sections showing immunoreactivity for α -SMA (A) and $\alpha_v\beta_5$ (B). Spindle-shaped cells within this fibrotic region were positive for both proteins. (C and D) Photomicrographs of representative 3- μ m serial paraffin sections showing immunoreactivity for α -SMA (C) and PAR1 (D). Again, spindle-shaped cells within a fibrotic region of IPF lung were positive for both markers. Scale bars: 100 μ m.

binds to the LSKL sequence of LAP, and this interaction can be blocked with peptides corresponding to the LSKL sequence (37). In our experiments, addition of LSKL peptides to the pHALF/tMLEC coculture attenuated TFLLR-induced tMLEC luciferase activity, but failed to block the induction of α -SMA protein in pHALFs in monoculture (data not shown). Taken together, these data suggest that TSP-1 blockade is not sufficient to block FXa-induced fibroblast-to-myofibroblast differentiation in pHALFs.

We therefore investigated an alternative, integrin-mediated mechanism of TGF- β activation; in fibroblasts, this process is thought to be predominantly mediated by the integrins $\alpha_v\beta_3$, $\alpha_v\beta_5$, and $\alpha_v\beta_8$ (36). In contrast to our data for TSP-1, addition of a neutralizing antibody to $\alpha_v\beta_5$ integrin completely blocked α -SMA induction by FXa (Figure 4, F and G). Because α -SMA induction was dependent on PAR1 coupling to the $G\alpha_q$ signaling pathway, and we had previously demonstrated that downstream of PAR1 activation, $G\alpha_q$ leads to Rho signaling in fibroblasts (32), we investigated the effect of the Rho kinase inhibitor Y-27632 on FXa-induced α -SMA expression. Y-27632 attenuated FXa-induced α -SMA accumulation in a concentration-dependent manner (Figure 4H), which indicates that this response is Rho kinase dependent.

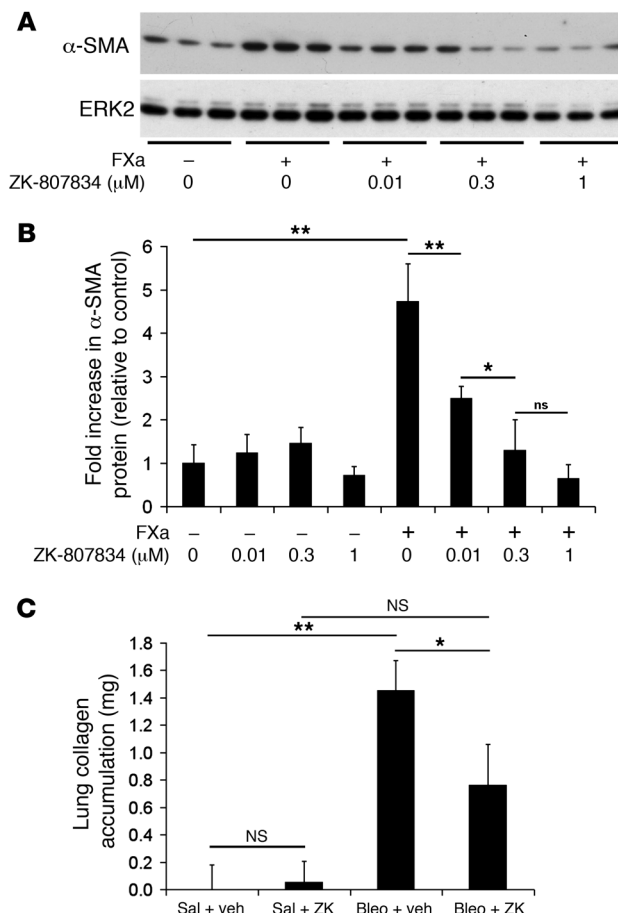
To confirm that $\alpha_v\beta_5$ integrin acts through TGF- β activation and/or signaling, we investigated whether neutralization of this integrin blocks FXa-induced SMAD2 phosphorylation. FXa-induced SMAD2 phosphorylation peaked at around 10 hours, and $\alpha_v\beta_5$ neutralization completely blocked this phosphorylation event (Figure 4, I and J). Consistent with a role for Rho kinase in mediating FXa-induced α -SMA accumulation, Y-27632 also inhibited

FXa-induced SMAD2 phosphorylation (data not shown). In contrast, the broad-spectrum MMP inhibitor GM 6001 (concentration range, 0.3–10 μ M) failed to abrogate either α -SMA induction or SMAD2 phosphorylation after FXa stimulation (data not shown), indicating that the $\alpha_v\beta_8$ and membrane type 1-MMP (MT1-MMP) mechanism is not involved. Taken together, these data indicate that FXa-induced fibroblast-to-myofibroblast differentiation is mediated via a TGF- β -dependent mechanism and that blockade of $\alpha_v\beta_5$ integrin and Rho kinase signaling inhibits this response.

To further explore the possibility that this integrin-mediated mechanism of TGF- β activation might be operative in human fibrotic lung disease, we assessed PAR1, $\alpha_v\beta_5$, and α -SMA immunolocalization in serial sections from the human IPF lung tissue of the Brompton cohort. Figure 5, A–D, shows that α -SMA and $\alpha_v\beta_5$ colocalized to fibrotic foci in serial cryostat sections of IPF lung (the antibody for $\alpha_v\beta_5$ was not compatible with paraffin sections). Both α -SMA and $\alpha_v\beta_5$ are expressed on cells with a typical spin-

Figure 6

Inhibition of FXa reduces bleomycin-induced lung fibrosis. (A and B) Effect of ZK 807834 on FXa-induced α -SMA protein expression in vitro. (A) Representative Western blot. (B) Densitometric analysis. Data are mean \pm SEM based on 3 replicates per group. (C) FXa inhibition attenuated lung collagen accumulation after bleomycin instillation in mice, as measured by reverse-phase HPLC quantitation of lung hydroxyproline in acid hydrolysates of pulverized lung. ZK, ZK 807834; veh, vehicle. Data are mean \pm SEM increase in lung collagen accumulation relative to the saline plus vehicle group. Values were obtained from groups of 6 (saline plus vehicle and bleomycin plus ZK 807834), 3 (saline plus ZK 807834), or 7 (bleomycin plus vehicle) mice. * P < 0.05, ** P < 0.001, ANOVA.





dle-shaped myofibroblast morphology. In serial paraffin sections from the same patients, α -SMA also colocalized with PAR1, again with significant expression within the fibrotic foci. Of interest, the $\alpha_v\beta_5$ integrin was also highly expressed on the smooth muscle layer underlying the larger airways and blood vessels (data not shown), suggesting that $\alpha_v\beta_5$ may also be important for the function of this related cell type. In concert with our immunohistochemical data on FX localization to fibrotic foci, these data support our *in vitro* model that FX signaling via PAR1 can lead to TGF- β activation by an $\alpha_v\beta_5$ -mediated mechanism, leading to fibroblast-myofibroblast differentiation in IPF.

Blocking FXa signaling attenuates bleomycin-induced lung fibrosis. The final aim of this study was to examine the contribution of FXa to the development of experimental pulmonary fibrosis by examining the effect of the direct FXa inhibitor ZK 807834 in the bleomycin model in mice. *In vitro* feasibility studies demonstrated that this compound completely blocked FXa-induced α -SMA protein expression in pHALFs (Figure 6, A and B), confirming the previously published observation that ZK 807834 is capable of inhibiting FXa cell signaling responses (38). Figure 6C shows the effect of this compound on lung collagen accumulation (as an index of fibrosis) at 14 days after bleomycin injury, when given daily by intraperitoneal injection from 24 hours onward: total lung collagen increased by 60% in bleomycin-injured mice compared with saline-instilled control animals. This increase was significantly reduced to 27% in bleomycin-injured mice given ZK 807834 (Figure 6C). In contrast, ZK 807834 had no effect on inflammatory cell recruitment in this model, since dosing for 5 days did not significantly reduce the total number of inflammatory cells in BALF (data not shown). These data confirm the importance of FXa in driving the fibrotic response in this mouse model.

Discussion

There is increasing evidence that uncontrolled activation of the coagulation cascade plays a pathophysiological role in numerous disease settings, including acute and chronic lung injury. It is generally held that coagulation zymogens are synthesized in the liver (26, 39) and are locally activated in response to tissue injury as a result of vascular leak and extravascular TF expression. The present study challenges this concept and proposes an additional mechanism for the generation of FXa via local extravascular expression of FX.

The observation that the gene encoding FX was expressed in the injured lung in this study was initially identified by microarray analysis of lung RNA from bleomycin-injured mice. This finding was validated by real-time RT-PCR of mouse lung homogenates and immunohistochemistry of tissue sections. Human disease relevance was confirmed by laser-capture microdissection of alveolar septae, which demonstrated marked upregulation of FX mRNA levels in IPF patients. Immunohistochemical analysis of tissue sections established that the bronchial and alveolar epithelia were prominent sites of FX/FXa immunoreactivity. We further demonstrated that bronchial and alveolar epithelial cells expressed FX at the mRNA level and that the FX band pattern observed by Western blotting was consistent with the posttranslational processing observed for FX in hepatocytes (26), which are classically viewed as the main cellular source of this zymogen. Interestingly, our gene chip studies further revealed that the enzymes γ -carboxylase and Vitamin K epoxide reductase (27) were expressed in the lung (data not shown). Moreover, of the profibrotic and proinflammatory mediators tested, only ROS were capable of substantially upregu-

lating FX mRNA levels in lung epithelial cells *in vitro* (Figure 2B). Lung tissues from IPF patients display elevated levels of markers of oxidative stress, while exhaled breath condensate contains increased levels of H₂O₂ (40). Experimental evidence suggests that oxidant/antioxidant imbalance may alter the pathogenesis of fibrotic lung diseases (41), and antioxidant therapy with N-acetylcysteine may show some promise in IPF (42). The action of ROS on the lung epithelium *in vivo* could therefore explain our observations of increased FX expression in IPF. Taken together, these data provide compelling evidence that the lung epithelium has the capacity to synthesize the mature 2-chain FX zymogen (43) and may represent a cellular source of this zymogen in the fibrotic lung.

The potential importance of a local cellular source of FX is further supported by our findings in the bleomycin model of lung fibrosis. Current dogma assumes that FX protein in the lung is derived solely from the circulating pool of FX through microvascular leak, rather than from local production. However, our data show that FXa activity in BALF was maintained at a significant level throughout both the inflammatory and the fibrotic phases of the bleomycin response, whereas microvascular leak was dramatically reduced during the fibrotic phase, in which, by inference, the leak of circulating coagulation zymogens is in decline. In contrast, local FX expression was significantly raised at 14 days. These findings support, albeit not unequivocally, that intra-alveolar FXa activity can potentially be maintained through the local generation of FX from the epithelium rather than from ongoing conversion of vascularly derived FX.

There is now good evidence that the extrinsic pathway of the coagulation cascade in the extravascular space is initiated by assembly of the TF/FVIIa/FX ternary complex leading to FXa activation (reviewed in ref. 44). It was previously reported that TF is absent in the normal lung, but is highly expressed by hyperplastic epithelial cells overlying fibrotic foci in patients with fibrotic lung disease (14), whereas FVII has previously been shown to be expressed and upregulated by alveolar macrophages isolated from patients with sarcoidosis (45). The present report shows that TF, FVII, and FX colocalize to the epithelium overlying fibrotic foci in IPF, so that FX is likely to be present at sites where it can be activated in the TF/FVIIa/FXa ternary complex. Moreover, FX/FXa also immunolocalizes to α -SMA-positive myofibroblasts within the fibrotic foci. We therefore propose a model whereby the TF/FVIIa/FX ternary complex assembles on the alveolar epithelium, allowing activation of FX to FXa that in turn influences fibroblast function within the underlying fibrotic regions.

Myofibroblasts are the primary effector cells in pulmonary fibrosis, responsible for producing the majority of matrix proteins within fibrotic foci (28). We report, for the first time to our knowledge, that activation of pHALFs by FXa *in vitro* promoted their differentiation into myofibroblasts. We further demonstrated that FXa mediated these effects via a PAR1- and TGF- β -dependent mechanism that was completely blocked with 2 mechanistically unrelated PAR1 antagonists and 2 structurally unrelated ALK5 inhibitors. Although FXa can signal via PAR1, PAR2, or both, depending on cell type and cofactor expression (9, 46), the data presented here adds further evidence that PAR1 plays a dominant role in FXa and fibroblast responses. Importantly, PAR1-deficient mice are protected from bleomycin-induced lung fibrosis (16). Our present findings contrast with a recent study in which a role for PAR2 in mediating FXa-induced myofibroblast differentiation is proposed (47).

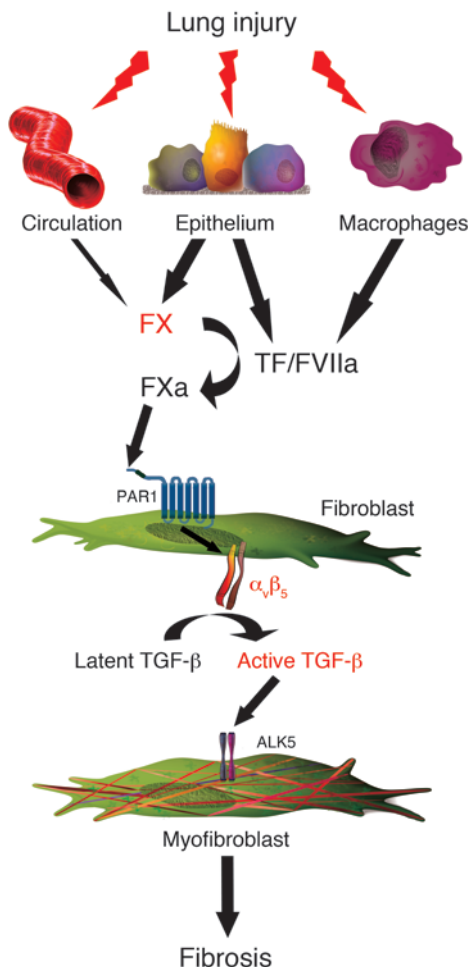


Figure 7
 Mechanism underlying the contribution of FX to lung fibrosis. After lung injury, both locally produced and circulation-derived FX contributes to increased FXa activity in the fibrotic lung. FXa induces its profibrotic effects via activation of PAR1 and subsequent differentiation of fibroblast into the myofibroblast phenotype. This is dependent on the activation of the $\alpha_v\beta_5$ integrin, leading to the activation of the major profibrotic cytokine TGF- β .

There are a number of potential explanations for these differences. First, the studies used different sources of fibroblasts: because our study was focused on the elucidation of pathomechanisms involved in lung fibrosis, we used pHALFs, while the prior report used murine myoblasts and a murine embryonic fibroblast cell line. Second, there are considerable differences in FXa concentrations. We used a standard concentration of 10 nM FXa, roughly 10-fold lower than that used by Borensztajn et al. (typically 1 U/ml, or 174 nM; ref. 47). Finally, it is interesting to note that PAR1-deficient mice are significantly protected from bleomycin-induced lung fibrosis (16), whereas PAR2-knockout mice have recently been shown not to be protected in murine models of fibrosis or acute lung injury (48). Thus, in the context of lung injury and fibrosis, current evidence suggests that PAR1 is the predominant coagulation signaling receptor involved. Moreover, although we previously hypothesized that thrombin is the major physiological activator of PAR1 in lung fibrosis (49), the data

presented here raise the possibility that locally produced and activated FX is an equally credible physiological activator of this receptor in the context of fibrotic lung disease.

The present study with FXa contrasts with the mechanism by which thrombin mediates myofibroblast differentiation via PAR1 activation in a TGF- β -independent manner, as proposed in other disease settings (50, 51). The difference between these previous reports and our present data with FXa – and, indeed, thrombin – may have several explanations, including the differences in thrombin concentrations, cell types, and TGF- β -blocking strategies. In our study, ALK5 inhibition completely blocked both FXa- and thrombin-mediated α -SMA induction. Interestingly, PAR1 is promiscuous in its ability to couple to multiple members of the G protein family, including $G\alpha_q$, $G\alpha_i$, and $G\alpha_{12/13}$, and different agonists of PAR1 have recently been shown to selectively activate different G protein pathways by their ability to alter receptor/G protein binding (52). Our data using the PAR1- $G\alpha_q$ antagonist Q94 revealed that $G\alpha_q$ signaling downstream of PAR1 activation was necessary for fibroblast-to-myofibroblast differentiation. Moreover, the attenuation of FXa-induced α -SMA induction with the Rho kinase inhibitor Y-27632 firmly places the Rho signaling pathway downstream of FXa in this response.

In this study, we further demonstrate a direct functional link between PAR1 signaling by FXa and the activation of latent TGF- β . Latent TGF- β activation represents a major rate-limiting step in the regulation of TGF- β bioavailability, and targeting this activation mechanism is currently a focus for the development of novel therapeutic strategies in IPF (28). The activation of latent TGF- β involves the conversion of the latent precursor to its biologically active form through dissociation from LAP. Several activation mechanisms have been described, including activation by integrin-dependent mechanisms (36) and interaction of the LAP with TSP-1 (37). Activation of TGF- β by integrins is dependent on the mechano-transduction of cytoskeletal tension within the fibroblast, in concert with matrix interactions, to change the conformation of the latent TGF- β complex (integrin-mediated traction model; ref. 36). Our present findings show that neutralization of the $\alpha_v\beta_5$ integrin blocked FXa-induced SMAD2 phosphorylation and α -SMA expression. Interfering with Rho signaling, a major pathway involved with actin assembly and cell contraction, also blocked FXa-induced SMAD2 phosphorylation and α -SMA induction. Taken together, these data provide compelling evidence for the $\alpha_v\beta_5$ integrin-mediated cell traction model in FXa/PAR1-induced TGF- β activation, and moreover demonstrate the importance of this pathway in the promotion of fibroblast-to-myofibroblast differentiation.

We provided evidence in vivo that $\alpha_v\beta_5$, α -SMA, and PAR1 were highly coexpressed by myofibroblasts within fibrotic foci in IPF lung sections. Such mechanisms of TGF- β activation are likely to be highly specific to fibroblasts within these regions, as $\alpha_v\beta_5$ staining was weak or absent on hyperplastic epithelial cells within the same tissue samples. There is good evidence that the $\alpha_v\beta_6$ integrin mechanism is the major activation mechanism involved in TGF- β activation by epithelial cells (53), so the absence of $\alpha_v\beta_5$ on the epithelium would be consistent with this alternative mode of TGF- β activation in this cell type. Because PAR1 ligation on epithelial cells can lead to the activation of TGF- β via an $\alpha_v\beta_6$ integrin-dependent mechanism (53), PAR1 activation on several cell types may play a pivotal role in driving the fibrotic response to lung injury. In terms of current drug targeting strategies in IPF, it is likely that blocking strategies targeting several TGF- β activation pathways will be required.



The final aim of this study was to determine whether FXa is causally involved in the development of experimental fibrosis by examining the effect of the direct inhibitor ZK 807834 in the bleomycin model of lung injury and fibrosis. This inhibitor was chosen on the basis that it inactivates both free FXa and FXa that is complexed with either TF/FVIIa or FVa (the prothrombinase complex). ZK 807834 is a highly specific direct inhibitor of FXa (K_i of 110 pM in vitro, compared with the 2- μ M K_i for thrombin; ref. 54) and has antithrombotic activity in experimental models of venous and arterial thrombosis (55, 56). In our present study, ZK 807834 was given at a dose known to result in appropriate bioavailability and pharmacokinetic parameters that lead to an increase in the partial thrombin time without affecting thrombin time – demonstrating specificity for FXa over thrombin in vivo. Lung collagen accumulation was significantly reduced in mice treated daily with this inhibitor from 24 hours after the initial bleomycin insult, indicating that FXa plays a significant role in the development of fibrosis in this model. Indirect inhibitors of FXa (57) have also been evaluated in the bleomycin model of lung injury in mice. For example, enoxaparin did not significantly reduce fibrosis, as determined by quantitative image analysis. However, given that the action of this drug is dependent on the presence of antithrombin, which is present in plasma, microvascular leak is required to maintain the inhibitory effect on FXa in the alveolar space. This may be particularly rate limiting during the fibrotic phase of the response, when microvascular leak is resolved but FX expression in the lung is at its peak. Moreover, indirect inhibitors are ineffective at blocking FXa in the TF/FVIIa/FXa ternary complex.

In conclusion, the findings of the present study provide compelling evidence that FXa, a central proteinase of the coagulation cascade, is locally produced in the injured lung and has the capacity to drive fibrotic responses to lung injury by activating TGF- β and influencing fibroblast-to-myofibroblast differentiation via a PAR1-dependent signaling mechanism (Figure 7). From a clinical perspective, it is increasingly recognized that therapeutic approaches based on direct FXa inhibition, rather than traditional, multitargeted anticoagulants (e.g., warfarin and unfractionated heparin), are likely associated with a wider therapeutic window and therefore reduced risk of bleeding complications (58, 59). We herein provide proof of principle that targeting FXa with a direct FXa inhibitor may be therapeutically beneficial. Our findings also have wider implications in the context of procoagulant signaling mechanisms: FXa, derived from a local tissue source rather than the circulation, may represent an important physiological activator of PAR1 in extravascular compartments. Finally, PAR1 is emerging as a critical receptor in the context of several fibrotic conditions, including those affecting the lung (16), liver (21), and kidney (60). The rationale for strategies aimed at blocking PAR1 signaling in fibrotic lung disease, and potentially other organs, is gaining strength.

Methods

Materials

Unless stated otherwise, reagents were purchased from Sigma-Aldrich. Bleomycin sulphate (trade name Bleo-Kyowa) was purchased from Kyowa Hakko. Human FXa was purchased from Enzyme Research Labs Ltd.; TGF- β 1 was from R&D Systems. The specific PAR1 agonist peptide TFLLR-NH₂ and the corresponding control peptide FTLLR-NH₂ were synthesized by R. Mecham (Washington University in St. Louis, St. Louis, Missouri, USA). The PAR2 agonist peptide SLIGKV-NH₂ was from Auspep. The selective

PAR1 antagonists RWJ-58259 and Q94 were prepared as described previously (30, 32). Q94 is a small molecule (MW 500) that meets the Lipinski rule of 5 and was identified during an ELISA screen, for competition of a high-affinity peptide that mimics the C terminus of G α_q , using a commercially available library (ChemDiv). A patent application for this compound has been filed (patent application EFS ID 2841714; application no. 61027665). The ALK5 inhibitor SD-208 was a gift from L.S. Higgins (Scios, Fremont, California, USA). The TSP-1-inhibitory peptide LSKL and the scrambled control peptide SLLK were a gift from J. Murphy-Ullrich (University of Alabama, Birmingham, Alabama, USA). The small-molecule FXa inhibitor ZK 807834 was previously described (61). The specific FXa inhibitor antistasin core peptide D-Arg32-Pro38 was purchased from Bachem. The FXa chromogenic substrate N- α -benzyloxycarbonyl-D-arginyl-L-glycyl-L-arginine-p-nitroaniline-dihydrochloride (S-2765) was purchased from Chromogenix. The broad-spectrum hydroxamic acid MMP inhibitor GM 6001 was purchased from Calbiochem. The highly specific ATP-competitive G-protein Rho-associated kinase inhibitor Y-27632 (K_i , 1.6 nM) was obtained from Calbiochem.

The antibodies used for Western blotting were as follows: mouse polyclonal anti- α -SMA (clone 1A4; Sigma-Aldrich); mouse monoclonal anti-TGF- β (clone 1D11; R&D Systems); rabbit polyclonal anti-FX (Santa Cruz Biotechnology Inc.); goat polyclonal anti-ERK2 (Santa Cruz Biotechnology Inc.); mouse polyclonal anti-TSP-1 (Neomarkers); and rabbit polyclonal anti-pSMAD2/3, rabbit polyclonal anti-SMAD2/3, and mouse monoclonal anti-SMAD2 (Cell Signaling Technology). Antibodies used for immunohistochemical localization studies were as follows: rabbit polyclonal anti-FX, as above; goat polyclonal anti-TSP-1 (Santa Cruz Biotechnology Inc.); rabbit polyclonal anti- α -SMA (Lab Vision); mouse monoclonal anti- α , β ₅ (clone P1F6; Abcam); mouse monoclonal anti-TF (clone 2K1; Abcam); mouse monoclonal anti-FVII/VIIa (clone CaFVII-22; Abcam); and rabbit polyclonal anti-TRED PAR1 (gift from E. Mackie, University of Melbourne, Melbourne, Victoria, Australia). Antibodies used for neutralization studies were mouse monoclonal anti- α , β ₅, as above, and mouse monoclonal IgG1 azide-free isotype (clone B-Z1; Abcam).

Animal models of pulmonary fibrosis

Oropharyngeal instillation of bleomycin. Male C57BL/6J mice (Harlan) were housed in a specific pathogen-free facility, and all procedures were performed on mice between 8 and 10 weeks of age. All animal studies were approved by the University College London Biological Services Ethical Review Committee and licensed under the Animals (Scientific Procedures) Act 1986 (Home Office, London, United Kingdom). Bleomycin (1 or 2 mg/kg body weight in 50 μ l saline) or saline was administered by oropharyngeal installation as described previously by Lakatos et al. (62) under light halothane-induced anesthesia.

For real-time RT-PCR and total lung collagen measurements, lungs were removed and blotted dry, and the trachea and major airways were excised before the separated lobes were snap frozen in liquid nitrogen. For histological and immunohistochemical analysis, the trachea was cannulated, and lungs were insufflated with 4% paraformaldehyde in PBS at a pressure of 25 cm H₂O, followed by removal of the heart and inflated lungs en bloc and immersion for 4 hours in fresh fixative. Subsequently, lungs were transferred to 15% sucrose in PBS and left overnight at 4°C before transfer to 70% ethanol.

FXa inhibition studies with ZK 807834. The in vivo contribution of FXa to lung collagen accumulation was investigated using the direct FXa inhibitor ZK 807834 (38, 61). At 24 hours after bleomycin administration, we began administration of ZK 807834 (50 mg/kg in acidified saline) or vehicle by intraperitoneal injection twice per day in the first week and once per day in the second week until the end of the 14-day experiment. The regimen



was chosen because this dosing gave a circulating concentration of ZK 807834 above 2 μM , which was sufficient to double the prothrombin time in C57BL/6J mice (data not shown). Mice were subsequently sacrificed, and total lung collagen was determined by measuring hydroxyproline content in aliquots of pulverized lung as described previously (16). Hydroxyproline was quantified by reverse-phase HPLC of 7-chloro-4-nitrobenzo-oxao-1,3,-diazole-derived acid hydrolysates; total lung collagen was then calculated in milligrams, and the data expressed as the lung collagen accumulation above baseline (i.e., saline-treated control mice).

During the course of the ZK 807834 experiment, 3 of 6 mice in the saline plus ZK 807834 group and 3 of 9 mice in the bleomycin plus ZK 807834 group were sacrificed as a result of intraperitoneal hemorrhage, arising from the multiple intraperitoneal injections. In addition, 1 of 8 mice in the bleomycin plus vehicle group was excluded from the HPLC analysis as an outlier because it did not display the characteristic loss of body weight after bleomycin instillation or the typical increase in lung weight.

Determination of microvascular leak. Plasma protein leakage into the alveolar space in the bleomycin model of fibrosis induced by oropharyngeal instillation of bleomycin was investigated at 7, 10, and 14 days after saline or bleomycin. Evans blue dye (EBD; 50 μl ; 10 mg/ml in 0.9% saline) was injected via the tail vein of C57BL/6J mice. The EBD was allowed to circulate for 1.5 hours, after which mice were sacrificed, and the thoracic cavity was exposed by dissection. Blood (400 μl) was withdrawn by cardiac puncture and mixed with 40 μl 3% sodium citrate. The pulmonary circulation was flushed with ice-cold 0.9% saline via the right ventricle, the trachea was cannulated, and BAL was performed using 3 0.5-ml aliquots of 0.9% saline. BALF was centrifuged at 400 g for 10 minutes at 4°C to remove cellular debris. The EBD concentration in plasma (separated from whole blood by centrifugation at 400 g for 10 minutes) and BALF were determined by measuring the absorbance at 620 nm on a spectrophotometer. The degree of microvascular leak was calculated as the ratio of [EBD] in BALF to [EBD] in plasma (expressed in AU).

Measurement of FXa concentration in BALF. FXa activity was determined using a commercially available spectrophotometric assay. Briefly, 100 μl of the BALF sample or FXa standard was incubated with 100 μl chromogenic substrate S-2765 (1.25 mg/ml) at 37°C. Absorbance was read on a spectrophotometer at 405 nm at regular intervals up to 30 minutes, and BALF active FXa concentration was derived by comparison of the initial rate ($\Delta\text{A}/\text{min}$) against the FXa standard curve. No activity was detectable in BALF from saline-treated animals. Total BALF protein concentration was measured using the bicinchoninic acid assay (Pierce Biotechnology). Active FXa levels were calculated as ng/mg total BALF protein.

Patient samples

Brompton cohort. Lung biopsy specimens were obtained from 7 patients with IPF (6 male, 1 female; mean age, 55.3 \pm 10.6; 6 specimens obtained at diagnostic surgical lung biopsy, 1 specimen obtained from lung explanted at transplant) and 6 control patients (4 male, 2 female; mean age, 65.3 \pm 15.8; obtained from cancer resection surgery of uninvolved tissue). All biopsies in this study were classified using the diagnostic criteria of the American Thoracic Society/European Respiratory Society consensus criteria: namely, a pattern of "usual interstitial pneumonia (UIP)" (63). Approval for the use of material was obtained from the Royal Brompton Harfield NHLI and the ethics committee of University College London and University College London Hospital. Informed consent was obtained from each subject.

Giessen cohort. Lung tissue biopsies were obtained from 10 patients with IPF (UIP pattern; 4 female, 6 male; mean age, 51.3 \pm 11.4 years) and 10 control subjects (organ donors; 5 female, 5 male; mean age, 47.5 \pm 13.9 years). The study protocol was approved by the Ethics Committee of the Justus-Liebig-University School of Medicine (AZ 31/93). Informed consent was obtained from each subject for the study protocol.

Pittsburgh cohort. Pittsburgh tissue microarrays (TMAs) were generated as previously described (64) from formalin-fixed, paraffin-embedded tissues stored at the University of Pittsburgh Tissue Bank at the Tissue Array Core facility. The TMAs included 12 samples with sarcoidosis, 7 samples with hypersensitivity pneumonitis, 18 samples with UIP, and 3 samples from head and neck tumors. Use of stored, deidentified tissues was approved by the University of Pittsburgh IRB.

Laser-capture microdissection

Microdissection was performed as described previously (65). In brief, 10- μm cryosections were mounted on glass slides, stained with hemalaun for 45 seconds, immersed in 70% and 96% ethanol, and stored in 100% ethanol until use. Alveolar septae were selected and microdissected using a laser MicroBeam system (P.A.L.M. Microlaser Technologies). The predominant epithelial phenotype was confirmed by differential expression pattern analysis of a panel of markers including cytokeratin, surfactant proteins C and A, CD45, PECAM, vimentin, α -SMA, and E-cadherin; macrophages were actively identified and removed from microdissected areas. Microdissected tissues were then transferred into reaction tubes containing 200 μl RNA lysis buffer, and samples were processed for RNA analysis, as described below.

Histological analysis and immunohistochemistry

For paraffin sections, individual lobes of mouse lungs or human biopsy material were placed in processing cassettes, dehydrated through a serial alcohol gradient, and embedded in paraffin wax blocks. For cryostat sections, snap-frozen biopsy material was embedded in OCT embedding matrix (Cellpath). Paraffin sections (3 μm) were cut and mounted on polylysine-coated glass slides before dewaxing in xylene and rehydration in ethanol according to standard histological procedures. Cryostat sections (3 μm) were cut and mounted on 3-aminopropyl-trioxysilane-coated (APES-coated) slides, air dried for 1 hour at room temperature, fixed in Zamboni fixative (1.5% picric acid in neutral-buffered paraformaldehyde) for 20 minutes, and washed for 5 minutes in TBS. Serial sections were cut with 3 μm separation. Antigens were unmasked by microwaving sections in 10 mM citrate buffer, pH 6.0 (2 10-minute washes for paraffin sections; 1 3-minute wash for cryostat sections) before washing in TBS and incubation with normal goat or rabbit serum (DAKO), as appropriate. For FVII, antigens were unmasked by incubating sections with proteinase K (20 $\mu\text{g}/\text{ml}$ in 10 mM Tris and 5 mM EDTA, pH 7.4) for 10 minutes at room temperature. Antigens were localized by overnight incubation with anti-FX (1:100 dilution), anti-TF (1:400 dilution), anti-FVII (1:170 dilution), anti-TSP-1 (1:250 dilution), anti-PAR1 (1:1,000 dilution), anti- α -SMA (1:400 dilution), or anti- $\alpha_v\beta_3$ (1:200 dilution) primary antibody. Serial cryostat sections were stained in the order α -SMA, $\alpha_v\beta_3$, α -SMA to maximize the likelihood of correctly colocalizing cells expressing both antigens. Sections were washed in TBS, incubated with a biotinylated goat anti-rabbit or rabbit anti-goat secondary antibody (1:200 dilution) for 1 hour, and washed again in TBS. Next, sections were incubated with a streptavidin/peroxidase complex (1:200 dilution; DAKO) for a further 30 minutes, followed by incubation with a 600- $\mu\text{g}/\text{ml}$ solution of 3,3'-diaminobenzidine tetrahydrochloride (Vector Laboratories) for color development. Sections were washed, counterstained with Gill-2 hematoxylin (Thermo-Shandon), dehydrated, and mounted with DPX mountant (Merck). Control sections were incubated with an isotype-specific, nonimmune rabbit, goat, or mouse IgG primary antibody (DAKO). Sections were then visualized by microscopy (DM5000B microscope; Leica Microsystems), and images were captured using a Qicam 12-bit color fast camera using Q capture software, version 2.81 (both from QImaging Corp.).



Table 1
Primers used for real-time RT-PCR

Gene	Forward	Reverse
Murine <i>F10</i>	5'-CAGCGGTTACTTCCTGGGTA-3'	5'-GCCACAGACCTTCTCTACG-3'
Human <i>F10</i>	5'-GCCCACTGTCTCTACCAAGC-3'	5'-CTTGATGACCACCTCCACCT-3'
Human <i>PAR1</i>	5'-CCATCGTTGTGTTTCATCCTG-3'	5'-GACCCAAACTGCCAATCACT-3'
Human <i>PAR2</i>	5'-CACCATCCAAGGAACCAATAG-3'	5'-TGCAGAAAACCTATCCACAGA-3'
Human <i>ACTA2</i>	5'-ATCCTGACTGAGCGTGGCTATT-3'	5'-GGCCATCTCATTTCCAAAGTCC-3'
Murine/human <i>18s</i>	5'-TTGACGGAAGGGCACCACCAG-3'	5'-GCACCACCACCCACGGAATCG-3'
Human <i>TSP1</i>	5'-CAATGAACGGGACAACCTGC-3'	5'-ATCTCCAATGCGGTCTGAGT-3'
Human <i>HPRT</i>	5'-GGCTTTGATTTTGTCTTTTCCA-3'	5'-AAGGACCCACGGAAGTGTG-3'

using the Applied Biosystems kit according to the manufacturer's instructions. Real-time RT-PCR was conducted using the Platinum SYBR Green qPCR SuperMix UDG (Invitrogen) on a LightCycler 1.5 Real-time Detection System (Roche) and analyzed using LightCycler Real-time PCR Detection System Software (version 3.5; Roche). Cycling conditions were as follows: 1 cycle of 50°C for 2 minutes and 95°C for 2 minutes; 45 cycles of 95°C for 5 seconds, 55°C for 5 seconds, and 72°C for 15 seconds. The specificity of the PCR product was confirmed by melting curve analysis and gel electrophoresis. For laser-capture microdissected samples, quantitative PCR was performed

Immunocytochemical visualization of actin fibers

Primary adult human lung fibroblasts were grown on chamber slides (Permanox, Nunclon; Fisher Scientific). Cells were washed with PBS and fixed in ice-cold methanol. The cell layer was washed twice with PBS before blocking nonspecific binding with normal goat serum for 1 hour at room temperature. After washing twice in PBS, primary anti- α -SMA antibody was added at a 1:50 dilution for 1 hour at room temperature. The cell layer was then incubated with secondary FITC-conjugated anti-mouse antibody (1:100 dilution; DAKO) for 30 minutes and washed twice with PBS before mounting using Vectashield (Vector Laboratories). Sections were visualized using a Zeiss Axioskop 2 microscope (Carl Zeiss Ltd.), and images were captured as described above.

Transcriptional profiling

cRNA was generated according to the instructions provided by Affymetrix. Briefly, total RNA from frozen powdered mouse lung tissue was isolated with TRIzol reagent according to the manufacturer's protocol (Invitrogen), DNase treated using a DNasefree kit (Ambion), and further purified by RNeasy Mini-kit (Qiagen). Double-stranded cDNA was synthesized using a Superscript Double-Stranded cDNA Synthesis kit (Invitrogen) according to the manufacturer's instructions, except that a T7-(dT)₂₄ oligonucleotide (5'-GGCCAGTGAATTGTAATACGACTACTATAGGGAGCGCGT₂₄-3') was used. cRNA was synthesized using the BioArray High Efficiency RNA Transcript Labeling kit (Enzo Life Sciences) and fragmented prior to microarray analysis using Affymetrix MOE430A GeneChips. These GeneChips contain 22,690 probe sets, corresponding to more than 14,000 genes. Expression measures were computed with Genespring GX software (version 7.3.1; Agilent Technologies) using GeneChip-robust multiarray averaging. The data discussed herein have been deposited in the NCBI Gene Expression Omnibus (66) and are accessible through GEO Series accession no. GSE16846 (<http://www.ncbi.nlm.nih.gov/geo/query/acc.cgi?acc=GSE16846>). Differential expression was assessed by filtering on fold change greater than 2 and statistical significance ($P < 0.05$ by Welch's t test, with Benjamini and Hochberg false discovery rate multiple testing correction). Gene ontology data mining for biological process at level 3 using Expression Analysis Systematic Explorer (EASE) software was used to determine statistical overrepresentation ($P < 0.05$ by Fisher exact test) of gene categories; analysis was conducted using the Database for Annotation, Visualization, and Integrated Discovery (DAVID) Tools (<http://david.abcc.ncifcrf.gov> and ref. 67).

Real-time RT-PCR analysis

Total RNA from frozen powdered lung tissue or cell cultures was isolated with TRIzol reagent per the manufacturer's protocol (Invitrogen). RNA was DNase treated using a DNasefree kit (Ambion). Random hexamers were used as the primer for RT of 1 μ g total RNA in a reaction volume of 20 μ l

using Sequence Detection System 7700 (Applied Biosystems). For each gene, crossing point (Cp) values were determined from the linear region of the amplification plot and normalized by subtraction of the Cp value for 18S or hypoxanthine-guanine phosphoribosyltransferase (HPRT) as appropriate, generating the Δ Cp value. Relative change was determined by subtraction of the Δ Cp value for the control sample from the Δ Cp value for the stimulated/fibrotic sample, giving the $\Delta\Delta$ Cp value. Fold change was subsequently calculated using the formula $2^{-\Delta\Delta C_p}$. Primers are shown in Table 1.

Cell culture

pHALFs grown from explant cultures of normal lung tissue were a gift from R.J. McAnulty (University College London). tMLECs stably expressing firefly luciferase under the control of a TGF- β -sensitive portion of the PAI-1 promoter were a gift from D. Rifkin (New York University, New York, New York, USA). A549 alveolar epithelial cells, BEAS-2B bronchial epithelial cells, HFL-1 human fetal lung fibroblasts, and the HepG2 hepatocyte cell line were purchased from the American Type Culture Collection. MLFs were a gift from S. Coughlin (UCSF, San Francisco, California, USA).

pHALFs were used below passage 10; A549, BEAS-2B, HFL-1, MLF, and HepG2 cells were used at passages below 20. pHALFs and HFL-1, MLF, and HepG2 cells were maintained in DMEM at 37°C (10% CO₂) supplemented with penicillin, streptomycin, and 10% (v/v) FBS (all from Invitrogen). BEAS-2B cells were grown in Optimem at 37°C (10% CO₂) supplemented with penicillin (200 U/ml), streptomycin (200 U/ml), glutamine (4 mM), and 10% (v/v) newborn calf serum. A549 cells were grown in F12 Kaign medium at 37°C (5% CO₂) supplemented with penicillin (200 U/ml), streptomycin (200 U/ml), glutamine (4 mM) and 10% (v/v) FBS. Cells were routinely passaged and tested for mycoplasma infection.

For stimulation of A549 cells with H₂O₂, cells were seeded at 2×10^5 cells/well in 6-well plates, allowed to adhere overnight, and then serum starved for 3 hours prior to stimulation with 400 μ M H₂O₂ for 1 hour, after which RNA was isolated using TRIzol (Invitrogen).

Western blot analysis of FX, α -SMA, pSMAD2/3; SMAD2, TSP-1 and ERK2

α -SMA, pSMAD2/3, and TSP-1 expression were analyzed by Western blotting. Cells were seeded at 1.5×10^5 cells/well in 12-well plates, grown to subconfluence, and allowed to quiesce in serum-free medium for 24 hours before exposure to control medium, 10 nM FXa, or 10 nM thrombin, with or without various inhibitors as indicated in the figure legends. After incubation, cells were washed with ice-cold PBS, then lysed on ice in 100 μ l of buffer containing 50 mM Tris, 150 mM NaCl, 20 mM NaF, 1 mM NaVO₃, 1 mM EDTA, 1 μ M PMSF, glycerol, 1% v/v Triton X-100, 0.1% w/v sodium dodecyl sulfate, and protease inhibitor cocktail (Roche). For studies of endogenous FX production by A549, BEAS-2B, and HepG2



cells, these cells were seeded at 2×10^5 cells/well in 6-well plates, allowed to adhere overnight, then washed with ice-cold PBS prior to protein lysis, as described above. Total protein was measured using the bicinchoninic acid assay (Pierce Biotechnology). Equal amounts of protein were loaded onto 10% SDS-PAGE gels, electrophoresed, transferred to nitrocellulose membranes (Hybond-ECL; Amersham Biosciences), and incubated with blocking buffer containing 5% nonfat dry milk in 50 mM Tris, 150 mM NaCl, 0.1% Tween-20, pH 7.4 (TBST) for 1 hour. Blots were then incubated with anti- α -SMA, anti-pSMAD2/3, anti-TSP-1, or anti-FX antibodies at 1:1,000 dilution in 5% BSA (w/v) in TBST overnight at 4°C. All blots were then washed with TBST and incubated for 1 hour at room temperature with HRP-conjugated secondary antibody. After further washing in TBST, immunoreactive bands were visualized by standard chemiluminescence (ECL reagent; Amersham Biosciences) according to the manufacturer's instructions. For examination of total ERK2 and SMAD2 levels (as loading controls), the blots were stripped using Restore stripping buffer (Pierce Biotechnology) for 30 minutes at room temperature before immunoblotting with anti-total ERK2 or anti-total SMAD2 antibodies using the protocol described above. Blots were scanned on an Epson Perfection 4870 photo scanner, and densitometric analysis was performed using NIH Image (version 1.63; <http://rsb.info.nih.gov/nih-image>) calibrated against Kodak photographic step tablet no. 3.

tMLEC assay

pHALFs and tMLECs were harvested by trypsinization, mixed at a 1:1 ratio, seeded at 4×10^4 cells/ml in DMEM supplemented with 10% (v/v) FBS in 48-well plates, and allowed 24 hours of incubation for adhesion and cell spreading. This medium was then changed to serum-free DMEM containing TFLLR or FTLR (200 μ M each) supplemented with anti-TGF- β antibody 1D11 (100 μ g/ml), LSKL or SLLK (10 μ M), or anti- $\alpha_v\beta_5$ anti-

body. The coculture proceeded overnight, and cells were washed once in PBS before cell lysis for 20 minutes at 4°C in reporter lysis buffer (Roche). The cell layer was agitated with a pipette and centrifuged at 1,500 g for 5 minutes at 4°C. The supernatant was added to luciferin assay buffer (Promega), and luminescence was measured at 24°C in a GENios Pro microplate reader (Tecan UK Ltd.).

Statistics

Statistical analyses were performed using 2-sample, 2-tailed, equal variance Student's *t* test or 1- or 2-way ANOVA with Student-Newman-Keuls post-hoc analysis. *P* values less than 0.05 were considered significant.

Acknowledgments

We thank Steve E. Bottoms and Danielle Copeman for expert technical assistance with immunohistochemistry. The research leading to these results has received funding from the Wellcome Trust (GR071124MA); the MBPhD programme of University College London; the Rockefeller Fund; the British Lung Foundation (F07/6); the Medical Research Council (G0800340); and the European Community's Seventh Framework Programme (FQ7/2007-2013) under grant agreement no. HEALTH-F2-2007-202224 eurIPFnet.

Received for publication July 16, 2007, and accepted in revised form June 3, 2009.

Address correspondence to: Rachel C. Chambers, Centre for Respiratory Research, University College London, Rayne Institute, 5 University Street, London WC1E 6JJ, United Kingdom. Phone: 44-207679-6978; Fax: 44-207679-6973; E-mail: r.chambers@ucl.ac.uk.

1. Contrino, J., Hair, G., Kreutzer, D.L., and Rickles, F.R. 1996. In situ detection of tissue factor in vascular endothelial cells: correlation with the malignant phenotype of human breast disease. *Nat. Med.* **2**:209–215.
2. Matetzky, S., et al. 2000. Smoking increases tissue factor expression in atherosclerotic plaques: implications for plaque thrombogenicity. *Circulation.* **102**:602–604.
3. Idell, S., et al. 1987. Procoagulant activity in bronchoalveolar lavage in the adult respiratory distress syndrome. Contribution of tissue factor associated with factor VII. *Am. Rev. Respir. Dis.* **136**:1466–1474.
4. Sapru, A., Wiemels, J.L., Witte, J.S., Ware, L.B., and Matthay, M.A. 2006. Acute lung injury and the coagulation pathway: Potential role of gene polymorphisms in the protein C and fibrinolytic pathways. *Intensive Care Med.* **32**:1293–1303.
5. Anthoni, C., et al. 2007. Tissue factor: a mediator of inflammatory cell recruitment, tissue injury, and thrombus formation in experimental colitis. *J. Exp. Med.* **204**:1595–1601.
6. Chambers, R.C. 2008. Procoagulant signalling mechanisms in lung inflammation and fibrosis: novel opportunities for pharmacological intervention? *Br. J. Pharmacol.* **153**:S367–S378.
7. Ossovskaya, V.S., and Bunnett, N.W. 2004. Protease-activated receptors: contribution to physiology and disease. *Physiol. Rev.* **84**:579–621.
8. Ruf, W., Dorfleutner, A., and Riewald, M. 2003. Specificity of coagulation factor signaling. *J. Thromb. Haemost.* **1**:1495–1503.
9. Blanc-Brude, O.P., et al. 2005. Factor Xa stimulates fibroblast procollagen production, proliferation, and calcium signaling via PAR1 activation. *Exp. Cell Res.* **304**:16–27.
10. Camerer, E., Kataoka, H., Kahn, M., Lease, K., and Coughlin, S.R. 2002. Genetic evidence that protease-activated receptors mediate factor Xa signaling in endothelial cells. *J. Biol. Chem.* **277**:16081–16087.
11. Ohba, T., et al. 1994. Scleroderma bronchoalveolar lavage fluid contains thrombin, a mediator of human lung fibroblast proliferation via induction of platelet-derived growth factor alpha-receptor. *Am. J. Respir. Cell Mol. Biol.* **10**:405–412.
12. Hernandez Rodriguez, N.A., et al. 1995. Role of thrombin in pulmonary fibrosis. *Lancet.* **346**:1071–1073.
13. Marshall, R.P., et al. 2000. Fibroproliferation occurs early in the acute respiratory distress syndrome and impacts on outcome. *Am. J. Respir. Crit. Care Med.* **162**:1783–1788.
14. Imokawa, S., et al. 1997. Tissue factor expression and fibrin deposition in the lungs of patients with idiopathic pulmonary fibrosis and systemic sclerosis. *Am. J. Respir. Crit. Care Med.* **156**:631–636.
15. Kubo, H., et al. 2005. Anticoagulant therapy for idiopathic pulmonary fibrosis. *Chest.* **128**:1475–1482.
16. Howell, D.C., et al. 2005. Absence of proteinase-activated receptor-1 signaling affords protection from bleomycin-induced lung inflammation and fibrosis. *Am. J. Pathol.* **166**:1353–1365.
17. Bogatkevich, G.S., et al. 2005. Distinct PKC isoforms mediate cell survival and DNA synthesis in thrombin-induced myofibroblasts. *Am. J. Physiol. Lung Cell Mol. Physiol.* **288**:L190–L201.
18. Howell, D.C., et al. 2001. Direct thrombin inhibition reduces lung collagen, accumulation, and connective tissue growth factor mRNA levels in bleomycin-induced pulmonary fibrosis. *Am. J. Pathol.* **159**:1383–1395.
19. Yasui, H., et al. 2001. Intratracheal administration of activated protein C inhibits bleomycin-induced lung fibrosis in the mouse. *Am. J. Respir. Crit. Care Med.* **163**:1660–1668.
20. Gunther, A., et al. 2003. Prevention of bleomycin-induced lung fibrosis by aerosolization of heparin or urokinase in rabbits. *Am. J. Respir. Crit. Care Med.* **168**:1358–1365.
21. Fiorucci, S., et al. 2004. PAR1 antagonism protects against experimental liver fibrosis. Role of proteinase receptors in stellate cell activation. *Hepatology.* **39**:365–375.
22. Lemay, A.M., and Haston, C.K. 2005. Bleomycin-induced pulmonary fibrosis susceptibility genes in AcB/BcA recombinant congenic mice. *Physiol. Genomics.* **23**:54–61.
23. Haston, C.K., Tomko, T.G., Godin, N., Kerckhoff, L., and Hallett, M.T. 2005. Murine candidate bleomycin induced pulmonary fibrosis susceptibility genes identified by gene expression and sequence analysis of linkage regions. *J. Med. Genet.* **42**:464–473.
24. Kaminski, N., et al. 2000. Global analysis of gene expression in pulmonary fibrosis reveals distinct programs regulating lung inflammation and fibrosis. *Proc. Natl. Acad. Sci. U. S. A.* **97**:1778–1783.
25. Katsuma, S., et al. 2001. Molecular monitoring of bleomycin-induced pulmonary fibrosis by cDNA microarray-based gene expression profiling. *Biochem. Biophys. Res. Commun.* **288**:747–751.
26. Stanton, C., and Wallin, R. 1992. Processing and trafficking of clotting factor X in the secretory pathway. Effects of warfarin. *Biochem. J.* **284**:25–31.
27. Rost, S., et al. 2004. Mutations in VKORC1 cause warfarin resistance and multiple coagulation factor deficiency type 2. *Nature.* **427**:537–541.
28. Scotton, C.J., and Chambers, R.C. 2007. Molecular targets in pulmonary fibrosis: The myofibroblast in focus. *Chest.* **132**:1311–1321.
29. Ohta, N., Brush, M., and Jacobs, J.W. 1994. Interaction of antistasin-related peptides with factor Xa: identification of a core inhibitory sequence. *Thromb. Haemost.* **72**:825–830.
30. Zhang, H.C., et al. 2001. Discovery and optimization of a novel series of thrombin receptor (par-1)



- antagonists: potent, selective peptide mimetics based on indole and indazole templates. *J. Med. Chem.* **44**:1021–1024.
31. Derian, C.K., et al. 2003. Blockade of the thrombin receptor protease-activated receptor-1 with a small-molecule antagonist prevents thrombus formation and vascular occlusion in nonhuman primates. *J. Pharmacol. Exp. Ther.* **304**:855–861.
32. Deng, X.L., et al. 2008. Thrombin induces fibroblast CCL2/JE production and release via coupling of PAR(1) to G alpha(q) and cooperation between ERK1/2 and Rho kinase signaling pathways. *Mol. Biol. Cell.* **19**:2520–2533.
33. Hu, B., Wu, Z., and Phan, S.H. 2003. Smad3 mediates transforming growth factor-beta-induced alpha-smooth muscle actin expression. *Am. J. Respir. Cell Mol. Biol.* **29**:397–404.
34. Abe, M., et al. 1994. An assay for transforming growth factor-beta using cells transfected with a plasminogen activator inhibitor-1 promoter-luciferase construct. *Anal. Biochem.* **216**:276–284.
35. Murphy-Ullrich, J.E., and Poczatek, M. 2000. Activation of latent TGF-beta by thrombospondin-1: mechanisms and physiology. *Cytokine Growth Factor Rev.* **11**:59–69.
36. Wipff, P.J., and Hinz, B. 2008. Integrins and the activation of latent transforming growth factor [beta]1 — An intimate relationship. *Eur. J. Cell Biol.* **87**:601–615.
37. Young, G.D., and Murphy-Ullrich, J.E. 2004. Molecular interactions that confer latency to transforming growth factor-beta. *J. Biol. Chem.* **279**:38032–38039.
38. McLean, K., Schirm, S., Johns, A., Morser, J., and Light, D.R. 2001. FXa-induced responses in vascular wall cells are PAR-mediated and inhibited by ZK-807834. *Thromb. Res.* **103**:281–297.
39. Miao, C.H., Leytus, S.P., Chung, D.W., and Davie, E.W. 1992. Liver-specific expression of the gene coding for human factor X, a blood coagulation factor. *J. Biol. Chem.* **267**:7395–7401.
40. Psathakis, K., et al. 2006. Exhaled markers of oxidative stress in idiopathic pulmonary fibrosis. *Eur. J. Clin. Invest.* **36**:362–367.
41. Kinnula, V.L., Fattman, C.L., Tan, R.J., and Oury, T.D. 2005. Oxidative stress in pulmonary fibrosis: a possible role for redox modulatory therapy. *Am. J. Respir. Crit. Care Med.* **172**:417–422.
42. Demedts, M., et al. 2005. High-dose acetylcysteine in idiopathic pulmonary fibrosis. *N. Engl. J. Med.* **353**:2229–2242.
43. Furie, B., and Furie, B.C. 1988. The molecular basis of blood coagulation. *Cell.* **53**:505–518.
44. Riewald, M., and Ruf, W. 2002. Orchestration of coagulation protease signaling by tissue factor. *Trends Cardiovasc. Med.* **12**:149–154.
45. Chapman, H.A., Jr., Allen, C.L., Stone, O.L., and Fair, D.S. 1985. Human alveolar macrophages synthesize factor VII in vitro. Possible role in interstitial lung disease. *J. Clin. Invest.* **75**:2030–2037.
46. Riewald, M., and Ruf, W. 2001. Mechanistic coupling of protease signaling and initiation of coagulation by tissue factor. *Proc. Natl. Acad. Sci. U. S. A.* **98**:7742–7747.
47. Borensztajn, K., et al. 2008. Factor Xa stimulates proinflammatory and profibrotic responses in fibroblasts via protease-activated receptor-2 activation. *Am. J. Pathol.* **172**:309–320.
48. Su, X., and Matthay, M.A. 2009. Role of protease activated receptor 2 in experimental acute lung injury and lung fibrosis. *Anat. Rec. (Hoboken)*. **292**:580–586.
49. Howell, D.C., Laurent, G.J., and Chambers, R.C. 2002. Role of thrombin and its major cellular receptor, protease-activated receptor-1, in pulmonary fibrosis. *Biochem. Soc. Trans.* **30**:211–216.
50. Bogatkevich, G.S., Tourkina, E., Silver, R.M., and Ludwicka-Bradley, A. 2001. Thrombin differentiates normal lung fibroblasts to a myofibroblast phenotype via the proteolytically activated receptor-1 and a protein kinase C-dependent pathway. *J. Biol. Chem.* **276**:45184–45192.
51. Zhang, A.W., et al. 2005. YB-1 coordinates vascular smooth muscle alpha-actin gene activation by transforming growth factor beta 1 and thrombin during differentiation of human pulmonary myofibroblasts. *Mol. Biol. Cell.* **16**:4931–4940.
52. McLaughlin, J.N., et al. 2005. Functional selectivity of G protein signaling by agonist peptides and thrombin for the protease-activated receptor-1. *J. Biol. Chem.* **280**:25048–25059.
53. Jenkins, R.G., et al. 2006. Ligand of protease-activated receptor 1 enhances alpha(v)beta6 integrin-dependent TGF-beta activation and promotes acute lung injury. *J. Clin. Invest.* **116**:1606–1614.
54. Light, D.R., and Guilford, W.J. 2001. Discovery of the factor Xa inhibitor, ZK 807834 (CI-1031). *Curr. Top. Med. Chem.* **1**:121–136.
55. Abendschein, D.R., et al. 2000. Effects of ZK-807834, a novel inhibitor of factor Xa, on arterial and venous thrombosis in rabbits. *J. Cardiovasc. Pharmacol.* **35**:796–805.
56. Karnicki, K., et al. 2004. Inhibition and reversal of platelet-rich arterial thrombus in vivo: direct vs. indirect factor Xa inhibition. *J. Thromb. Haemost.* **2**:2162–2169.
57. Laxer, U., et al. 1999. The effect of enoxaparin on bleomycin-induced lung injury in mice. *Exp. Lung Res.* **25**:531–541.
58. Hirsh, J., O'Donnell, M., and Weitz, J.I. 2005. New anticoagulants. *Blood.* **105**:453–463.
59. Bauer, K.A. 2006. New anticoagulants: anti IIa vs anti Xa—is one better? *J. Thromb. Thrombolysis.* **21**:67–72.
60. Cunningham, M.A., et al. 2000. Protease-activated receptor 1 mediates thrombin-dependent, cell-mediated renal inflammation in crescentic glomerulonephritis. *J. Exp. Med.* **191**:455–462.
61. Phillips, G.B., et al. 1998. Discovery of N-[2-[5-[Amino(imino)methyl]-2-hydroxyphenoxy]-3,5-difluoro-6-[3-(4,5-dihydro-1-methyl-1H-imidazol-2-yl)phenoxy]pyridin-4-yl]-N-methylglycine (ZK-807834): a potent, selective, and orally active inhibitor of the blood coagulation enzyme factor Xa. *J. Med. Chem.* **41**:3557–3562.
62. Lakatos, H.F., et al. 2006. Oropharyngeal aspiration of a silica suspension produces a superior model of silicosis in the mouse when compared to intratracheal instillation. *Exp. Lung Res.* **32**:181–199.
63. American Thoracic Society, European Respiratory Society. 2002. American Thoracic Society/European Respiratory Society international multidisciplinary consensus classification of the idiopathic interstitial pneumonias. This joint statement of the American Thoracic Society (ATS), and the European Respiratory Society (ERS) was adopted by the ATS board of directors, June 2001 and by the ERS executive committee, June 2001. *Am. J. Respir. Crit. Care Med.* **165**:277–304.
64. Kajdacsy-Balla, A., et al. 2007. Practical aspects of planning, building, and interpreting tissue microarrays: The Cooperative Prostate Cancer Tissue Resource experience. *J. Mol. Histol.* **38**:113–121.
65. Fink, L., et al. 1998. Real-time quantitative RT-PCR after laser-assisted cell picking. *Nat. Med.* **4**:1329–1333.
66. Edgar, R., Domrachev, M., and Lash, A.E. 2002. Gene Expression Omnibus: NCBI gene expression and hybridization array data repository. *Nucleic Acids Res.* **30**:207–210.
67. Dennis, G., Jr., et al. 2003. DAVID: Database for Annotation, Visualization, and Integrated Discovery. *Genome Biol.* **4**:P3.